Food Chemistry 210 (2016) 491–499

Contents lists available at ScienceDirect

Food Chemistry

journal homepage: www.elsevier.com/locate/foodchem

Limited proteolysis of myoglobin opens channel in ferrochelatase-globin complex for iron to zinc transmetallation

Marcella O. Paganelli [a], Alberto B. Grossi [b], Paulo R. Dores-Silva [a], Julio C. Borges [a], Daniel R. Cardoso [a,*], Leif H. Skibsted [b,*]

[a] Instituto de Química de São Carlos, Universidade de São Paulo, Avenida Trabalhador São Carlense 400, CP 780, 13560-470 São Carlos, Brazil
[b] Food Chemistry, Department of Food Science, University of Copenhagen, Rolighedsvej 30, DK-1958 Frederiksberg C, Denmark

ARTICLE INFO

Article history:
Received 21 September 2015
Received in revised form 20 April 2016
Accepted 22 April 2016
Available online 23 April 2016

Keywords:
Parma ham
Ferrochelatase
Myoglobin
Meat pigment
Transmetallation

ABSTRACT

Recombinant ferrochelatase (BsFECH) from *Bacillus subtilis* expressed in *Escherichia coli* BL21(DE3) was found by UV-visible spectroscopy to bind the model substrate tetraphenylporphyrin-sulfonate, TPPS, with $K_a = 3.8\ 10^5$ mol/L in aqueous phosphate buffer pH 5.7 at 30 °C, and to interact with metmyoglobin with $K_a = 1.07 \pm 0.13\ 10^5$ mol/L at 30 °C. The iron/zinc exchange in myoglobin occurring during maturation of Parma hams seems to depend on such substrate binding to BsFECH and was facilitated by limited pepsin proteolysis of myoglobin to open a reaction channel for metal exchange still with BsFECH associated to globin. BsFECH increased rate of zinc insertion in TPPS significantly and showed saturation kinetics with an apparent binding constant of Zn(II) to the [enzyme-TPPS] complex of $1.3\ 10^4$ mol/L and a first-order rate constant of $6.6\ 10^{-1}\ s^{-1}$ for dissociation of the tertiary complex, a similar pattern was found for zinc/iron transmetallation in myoglobin.

© 2016 Elsevier Ltd. All rights reserved.

1. Introduction

Insertion of ferrous iron into protoporphyrin IX to produce protoheme is catalyzed by ferrochelatase (FECH; EC 4.99.1.1, protoheme ferrolyase) and is the terminal step in heme biosynthesis (Ajioka, Phillips, & Kushner, 2006; Ferreira et al., 1995). FECH genes have been isolated and sequenced from various organisms ranging from bacteria to higher eukaryotes and its catalytic residues are conserved. The prokaryotic and eukaryotic enzymes vary with regard to their cellular distribution and the presence or absence of an iron-sulfur cluster at the carboxyl terminal of the protein (Ajioka et al., 2006; Ferreira et al., 1995). The role of this cluster present in the mammalian enzyme is still unclear. Ferrous iron has been established as the preferential substrate for the enzyme *in vivo*. Although it was proved that FECH irreversibly catalyzes the insertion of metal ions into porphyrin ring, it was also demonstrated, *in vitro*, that FECH can catalyze iron removal from heme to create protoporphyrin and subsequently convert protoporphyrin IX to Zn-protoporphyrin IX (Chau, Ishigaki, Kataoka, & Taketani, 2010; Chau, Ishigaki, Kataoka, & Taketani, 2011; Taketani et al., 2007).

In dry cured meat products and in cooked hams the characteristic red color is usually due to nitrosylmyoglobin and nitrosylhemochromagen, respectively (Pegg & Shahidi, 1997). Because nitrosamines, generated in meat product upon addition of nitrite, are considered to be associated with cancer risk, nitrite free meat products are often preferred and considered to be a healthier alternative (Bryan, Alexander, Coughlin, Milkowski, & Boffetta, 2012; Mirvish, 1995). Parma hams are produced without the addition of nitrites but still develop a characteristic red color (Parolari, Benedini, & Toscani, 2009; Wakamatsu, Nishimura, & Hattori, 2004). The nature of the Parma ham pigment has been unexplained until 2004, when Zn-protoporphyrin IX was found to contribute to red color (Wakamatsu et al., 2004). Three possible mechanisms have been suggested for formation of the Parma ham pigment including a) a non-enzymatic reaction in which Zn-protoporphyrin is formed under anaerobic conditions (Becker, Westermann, Hansson, & Skibsted, 2012); b) enzymatic reactions where FECH is directly involved (Becker et al., 2012; Chau et al., 2011); c) bacterial enzymatic reactions (Morita, Niu, Sakata, & Nagata, 1996). We have recently suggested a novel mechanism by which Zn-protoporphyrin formation is promoted when myoglobin is partly degraded by endogenous peptidases during muscle salting and ham maturation (Grossi, do Nascimento, Cardoso, & Skibsted, 2014). The role of FECH at various stages of the degradation of myoglobin was not investigated and previously

* Corresponding authors.
E-mail addresses: drcardoso@iqsc.usp.br (D.R. Cardoso), ls@food.ku.dk (L.H. Skibsted).

http://dx.doi.org/10.1016/j.foodchem.2016.04.109
0308-8146/© 2016 Elsevier Ltd. All rights reserved.

non-enzymatic formation of Zn-protoporphyrin IX was suggested to occur in parallel with the enzymatic exchange reaction (Becker et al., 2012). It seems timely to explore how myoglobin degradation by proteolysis modulates transmetallation catalyzed by myoglobin as substrate for FECH and may further affect Zn-protoporphyrin IX formation. We now report the results of such investigations combining experiments with tetraphenylporphyrin sulfonate as a model substrate for kinetic studies and with partly proteolyzed myoglobin as substrate using recombinant *B. subtilis* FECH as the active enzyme. FECH from prokaryotic organisms is easily obtained for such model studies and may also form the basis for future use in the meat processing industry.

2. Material and methods

2.1. Protein expression and purification

Recombinant *Bacillus subtilis* ferrochelatase (BsFECH) carrying His-tag was obtained by inserting corresponding DNA into pET28a vector. The recombinant BsFECH was expressed by *Escherichia coli* BL21(DE3) strain cultivated in the LB medium containing 50 μg/L of Kanamycin. The cultures were induced using 0.4 mM of isopropyl β-D-1-thiogalactopyranoside (IPTG; Sigma-Aldrich, Steinheim, Germany) and incubated at 30 °C for 4 h. These cells were pelleted by centrifugation (7000 rpm at 4 °C for 30 min) and protein expression was checked by SDS-PAGE 12%. Pelletized bacteria were suspended in buffer added of 5 U of DNAse kit (Promega, Madison, WI) and 30 μg/L of lysozyme (Sigma-Aldrich, Steinheim, Germany) and incubated for 1 h in an ice-bath. Cells were then disrupted by ultrasonic cavitation and the soluble fractions separated by centrifugation (14,000 rpm at 4 °C for 30 min) and further analyzed by SDS-PAGE 12% gel stained with coomassie blue (Sigma-Aldrich, Steinheim, Germany). The recombinant BsFECH in the soluble fraction was purified by Ni^{2+} affinity chromatography using a HiTRAP chelating column in a Äkta Prime instrument (GE Healthcare Lifesciences, Uppsala, Sweden). The His-tagged protein was cleaved using 1U/mg thrombin (Sigma-Aldrich, Steinheim, Germany) for 12 h at 4 °C. Recombinant BsFECH was further purified by size-exclusion chromatography using a HiLoad Superdex 200pg 26/60 column coupled to a Äkta Prime instrument (GE Healthcare Lifesciences, Uppsala, Sweden) equilibrated with the 25 mM Tris-HCl buffer pH 7.5 (Sigma-Aldrich, Steinheim, Germany), 100 mM NaCl (Sigma-Aldrich, Steinheim, Germany) and 1 mM β-mercaptoethanol (Sigma-Aldrich, Steinheim, Germany). Protein concentration was determined by the absorbance of the protein solution at 280 nm according to established procedures in the literature (Edelhoch, 1967).

Recombinant BsFECH was studied by analytical size exclusion chromatography in order to estimate the Stokes radius as well as oligomeric status. For that, we used a Superdex 200 10/300 GL column (GE Healthcare Lifesciences, Uppsala, Sweden) coupled to a ÄKTA Prime device, equilibrated with the 25 mM Tris-HCl buffer (pH 7.5), 100 mM NaCl and 1 mM β-mercaptoethanol. The standard protein mixture was constituted by apoferritin (480 kDa/R_s 67 Å), γ-globulin (160 kDa/R_s 48 Å), BSA (67 kDa/R_s 36 Å), ovalbumin (45 kDa/R_s 29 Å), carbonic anhydrase (29 kDa/R_s 24 Å) and cytochrome C (12 kDa/R_s 14 Å) (Sigma-Aldrich, Steinheim, Germany). The retention times were transformed to the partition coefficient K_{av} applying the following equation:

$$K_{av} = \frac{V_e - V_o}{V_t - V_o} \quad (1)$$

where V_e is the elution volume of the protein; V_0 is the void volume of the column and the V_t is the total volume of the column. The $-\log K_{av}$ was plotted against the R_s of standards in order to estimate the R_s of BsFECH by linear regression. The frictional ratio (f/f_0) was estimated by the ratio of the experimental R_s to the radius of a sphere of the same mass.

2.2. Synchrotron small angle X-ray scattering

Small-angle X-ray scattering (SAXS) experiments were performed at the Brazilian Synchrotron Light Laboratory (LNLS, Campinas-SP, Brazil) using a monochromatic X-ray beam ($\lambda = 1.488$ Å) of the D02A-SAXS1 beam line. The sample-to-detector distance was ~1000 mm, which corresponds to the scattering vector range of $0.015 < q < 0.35$ Å^{-1}, where q is the magnitude of the q-vector defined by $q = (4\pi/\lambda)\sin\theta$ (2θ is the scattering angle). The protein samples were placed in a 1-mm path-length cell formed by two mica windows, and the scattering curves were recorded at 0.6 mg/mL in buffer solutions, as indicated below. The sample and buffers were subjected to X-ray frames of 100 s, and the scattering curves were corrected for the detector response and scaled by the incident beam intensity and the sample attenuation. The corrected scattering sample was subtracted from the scattering buffer curve. The Guinier law was used to estimate both protein radius of gyration (R_g) and irradiation intensity I(0). The GNOM program (Semenyuk & Svergun, 1991) was used to generate the pair distance distribution curves (p(r) curves), which supply information about protein size and shape.

2.3. UV-vis absorption spectroscopy and spectral titrations

Spectrophotometric titrations were carried out in an Shimadzu UV3600 spectrophotometer equipped with a TCC-100 Thermoelectrically Temperature Controlled Cell Holder (Shimadzu Co., Kyoto, Japan) and using 0.2 × 0.2 quartz cell (Hellma Gmbh, Müllheim, Germany) or using a 96-well plate reader spectrophotometer Multiskan GO (Thermo Scientific, Vartaa, Finland). The spectrophotometric studies of the metal exchange reactions were done using the same spectrophotometer with thermostated cell holder. The sodium tetraphenylporphyrin sulfonate, TPPS, and the zinc acetate used for the kinetic studies were from Sigma-Aldrich (Steinheim, Germany).

2.4. Circular dichroism (CD) spectroscopy

CD spectra were recorded in J-815 spectropolarimeter (Jasco Corp., Tokyo, Japan) coupled to the Peltier system PFD 425S for temperature control and using a quartz curvet of 1 mm × 1 mm (Hellma-Gmbh, Müllheim, Germany) for protein concentration of 0.17 mg/mL and of 0.5 mg/mL. CD spectra were normalized to the mean residue ellipticity ([θ]), and the protein secondary structure content was estimated using the CDNN deconvolution program (Bohm, Muhr, & Jaenicke, 1992). Half-denaturation concentrations (C_m) of urea as denaturant was determined by parameter fitting accordingly to the denaturation equilibrium:

$$\text{native} - \text{BsFECH} + \text{n urea} \rightleftharpoons \text{denaturated} - \text{BsFECH} \cdot (\text{urea})_n \quad (2)$$

with the following equilibrium expression:

$$K_{N\to D} = \frac{[denaturated - BsFECH \cdot (urea)n]}{[urea]^n * [native - BsFECH]} \quad (3)$$

$$\log \frac{[native - BsFECH]}{[denaturate - BsFECH \cdot (urea)n]} = \log K_{N\to D} + n * \log[urea] \quad (4)$$

Thermal-induced unfolding was monitored by CD spectroscopy and were performed with 1 mg/mL protein in a 1 mm quartz cuvette using a heating rate of 1 °C/min and data acquisition at

220 nm in 0.5 °C intervals. T_m, the temperature at the midpoint transition, was obtained by fitting the delta of signal data to a sigmoidal Boltzmann function.

2.5. Fluorescence spectroscopy

Fluorescence emission measurements were performed in an F-4500 fluorescence spectrophotometer (Hitachi High-Tech, Tokyo, Japan) using a 10 × 2-mm path-length cell (Hellma Gmbh, Müllheim, Germany) and thermostated at 25 °C.

2.6. Myoglobin digestion

Solutions containing 1 mM metmyoglobin (equine heart from Sigma-Aldrich, Steinheim, Germany) dissolved in purified H_2O were incubated with pepsin from porcine stomach mucosa (Sigma-Aldrich, Steinheim, Germany) (dissolved in 50 mM acetate buffer, pH 4.5) at 37.0 °C for varying times of proteolysis (from 5 min up to 90 min) (Carlsen & Skibsted, 2004). The myoglobin-to-pepsin ratio was approximately 90:1. The proteolytic reaction was chemically quenched at the defined incubation time by mixing equal volumes of 0.60 M $NaHCO_3$ (Sigma-Aldrich, Steinheim, Germany) and 0.10 M NaOH (Sigma-Aldrich, Steinheim, Germany) to the samples and the pH adjusted to neutral thereby inhibit further proteolysis. For all proteolyzed samples, pH was measured immediately after pepsin digestion and again after readjustment of pH to neutral conditions.

2.7. Liquid-chromatography electrospray ionization high-resolution accurate mass spectrometry

LC–ESI-MS separation were carried out in an Accela High Speed LC (Thermo Electron, San Jose, CA, USA) equipped with an Aeris XB-C18 column (15 cm × 2.1 mm × 3.6 μm; Phenomenex, Torrance, CA, USA) and using 0.1% aqueous formic acid:acetonitrile 1:1 v/v as mobile phase at a flow rate of 0.4 mL/min. Accurate high-resolution mass spectra were acquired in a FT-MS Orbitrap Velos mass spectrometer using an HESI-II interface (Thermo Electron, San Jose, CA, USA).

2.8. Isothermal titration calorimetry (ITC)

ITC experiments for probing the interaction between myoglobin and BsFECH were carried out using a MicroCal iTC_{200} instrument (GE Healthcare Lifesciences, Tokyo, Japan). The experiments were conducted using aqueous phosphate 100 mM buffer at pH 5.7 and ionic strength of 200 mM adjusted with NaCl. Proteins solution were dialyzed for 12 h against the same buffer. A total of 203.8 μL of BsFECH solution (30 μM) was titrated with a 500 μM metmyoglobin solution using 14 injections of 2.8 μL and injection time of 2.5 s with a waiting time of 120 s between each point; the exception was the first injection with a volume of 0.4 μL and a injection time of 0.8 s. Interaction experiment were carried out at three different temperatures (20 °C, 25 °C, and 30 °C) and the average heat of the last five titration points were used for heat of dilution correction.

3. Results and discussion

Ferrochelatase, FECH, from *B. subtilis* was expressed in *E. coli* BL21(DE3) and this recombinant FECH was added, after isolation and purification, as an exogenous enzyme to aqueous solutions of tetraphenylporphyrin sulfonate, TPPS, together with zinc acetate, as a model substrate and to partly proteolyzed solutions of ferrous myoglobin, as the substrates being formed in muscles during salting and in hams during maturation.

3.1. Characterization of Bacillus subtilis ferrochelatase

The recombinant enzyme was purified by Ni^{2+} affinity chromatography and by size-exclusion chromatography. Expression and the efficacy of BsFECH purification were monitored by 12% SDS-PAGE electrophoresis. It is clear from the 12% SDS-PAGE electropherogram that FECH was successfully expressed in its soluble form (Fig. S1A, Supplementary information). Analytical size-exclusion chromatography demonstrate that recombinant BsFECH displays an apparent molecular weight of 45 kDa, which is higher than the calculated molecular weight (37 kDa) suggesting an asymmetric monomer in solution (Fig. S1B, Supplementary information). Circular dichroism spectroscopy (CD) further shows that 32% and 18% of the protein had a α-helix and a β-sheet structures, respectively, in agreement with literature values (Greenfield, 2006). Data obtained from the analytical size-exclusion chromatography elution profile shows that the purified BsFECH had a Stokes radius of 30 Å compared to a an expected radius of 20 Å for a protein sphere of this molecular weight corresponding to frictional ratio of 1.4. The analytical size-exclusion chromatography data further confirm that BsFECH was an elongated monomer in solution in accordance with data obtained by SAXS (Al-Karadaghi, Hansson, Nikonov, Jonsson, & Hederstedt, 1997) (Figs. S1C, S1D, and S2, Supplementary information).

3.2. Stability of Bacillus subtilis ferrochelatase

BsFECH denaturation was investigated using CD and fluorescence spectroscopy (data not shown) and the two methods provide comparable results. Urea was used a chemical denaturant and as is seen from CD measurements, BsFECH is slightly more stable at physiological (pH 7.4) compared to the acidic conditions (pH 5.7) for urea as a chemical denaturant (Fig. S3, Supplementary information). Notably, NaCl protects BsFECH against denaturation as seen from the urea concentrations required for half-denaturation (Fig. S3, Supplementary information). A similar pattern is seen for thermal denaturation where salt increases the temperature requested for the equilibrium of half-denaturation. The protection of FECH structure by salt especially at physiological pH against chemical and thermal denaturation seems of importance for FECH activity in meat products during salting and maturation since a salt concentration of 7 up to 12% is usually employed in the manufacture process. Further, some structural parameters for recombinant BsFECH upon changing of pH (from 7.4 to 5.7) or by high salt concentration (up to 500 mM of NaCl) were monitored by SAXS technique, which shows that the gyration ratio (R_g) was not affected by those experimental conditions. The particle distance distribution function curves, p(r) curves, also suggested that the different experimental conditions tested did not change either shape or maximum particle distance (Fig. S2, Supplementary information). Besides, these structural parameters were in good accordance to those observed for crystallographic structure of *Bacillus subtilis* FECH (Al-Karadaghi et al., 1997) and indicated the elongated shape, as aforementioned.

3.3. Substrate binding to FECH

Tetraphenylporphyrin sulfonate, TPPS, was used as a water-soluble model substrate for BsFECH. UV-vis spectra of TPPS changed instantaneously upon addition of FECH as seen in Fig. 1A for solutions of BsFECH and TPPS without zinc(II) added.

It has been postulated that FECH plays a role during the catalytic reaction of transmetallation by forcing the porphyrin ring

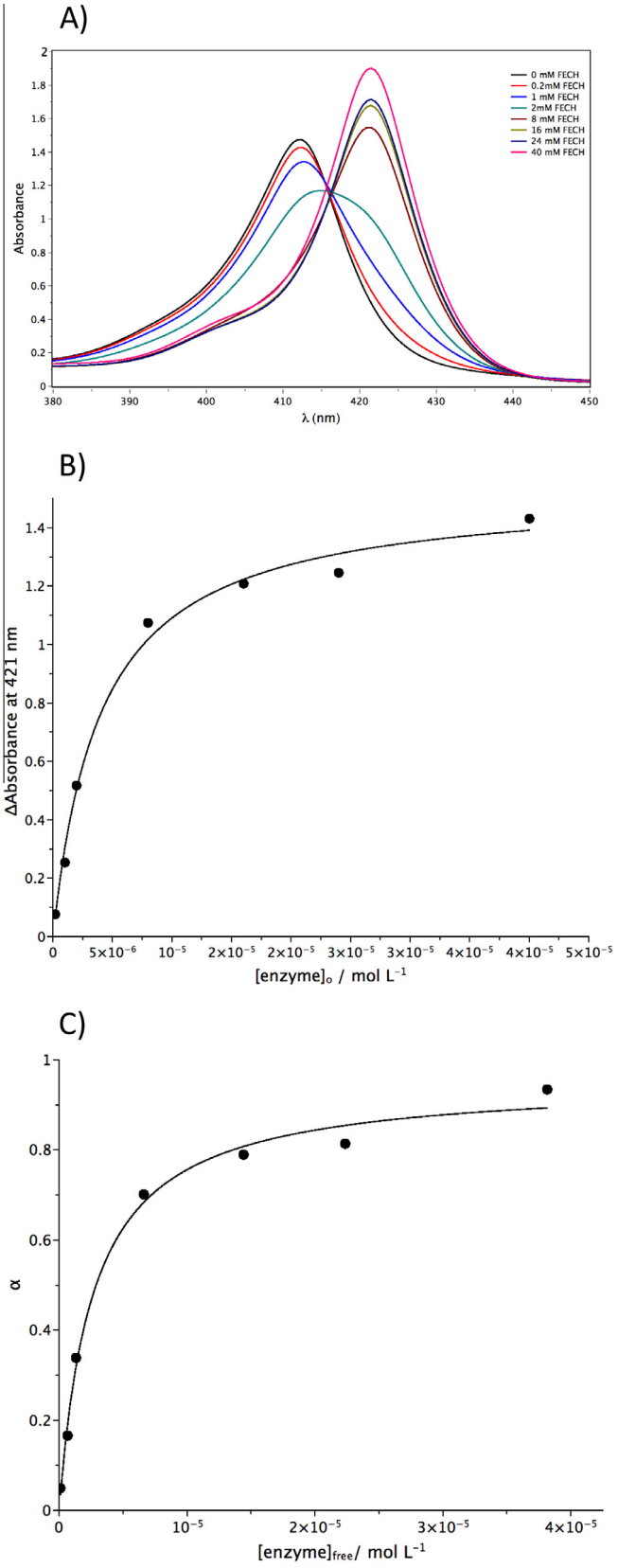

Fig. 1. Binding of tetraphenylporphyrin sulfonate, TPPS, to FECH as a model substrate in aqueous solution pH 5.7 at 30 °C. A) Spectral changes of TPPS (2.0 μM) for increasing concentrations of FECH. B) ΔAbsorbance at 421 nm for increasing concentration of FECH. C) Nonlinear plot of α *versus* the concentration of free FECH.

toward a distorted conformation in which the two-pyrrole nitrogen electrons are more accessible to the incoming metal ion substrate (Franco, Ma, Lu, Ferreira, & Shelnutt, 2000). Changes in the UV-vis absorption spectra as seen in Fig. 1 is a result of TPPS binding to BsFECH which may lead to the as ruffling or saddling of the porphyrin, as induced by FECH substrate (Franco et al., 2000). Red-shift of the soret band could also indicate transfer of the TPPS to a more hydrophobic environment, but confirm for both cases that the recombinant BsFECH purified in this study is active and capable of binding to the porphyrin ring and catalyzing the transmetallation reaction.

The spectral changes in the Soret-band region, as seen in Fig. 1A, provide information about binding stoichiometry and the stability constant for binding of TPPS to BsFECH in aqueous solution of pH 5.7 at 30 °C:

$$\mathrm{BsFECH} + \mathrm{nTPPS} \rightleftharpoons \mathrm{BsFECH(TPPS)_n} \tag{5}$$

$$K_a = \frac{[BsFECH(TPPS)n]}{[BsFECH] * [TPPS]^n} = \frac{1}{K_D} \tag{6}$$

and were analyzed accordingly to literature protocols (Barrios et al., 2014; Chenprakhon, Sucharitakul, Panijpan, & Chaiyen, 2010). The binding of TPPS to BsFECH was found to have a 1:1 stoichiometry corresponding to n = 1 in Eq. (5) and plotting ΔAbsorbance at 421 nm *versus* concentration of BsFECH provide a calculated ΔA_{max} which was in turn used to calculate α for the average ΔA for each BsFECH concentration, Fig. 1B. A nonlinear plot of α *versus* the concentration of free BsFECH (Fig. 1C) provided the value of the apparent binding constant ($K_a = 3.8 \cdot 10^5$ L/mol) according to:

$$\alpha = \frac{[\mathrm{BsFECH}]}{K_D + [\mathrm{BsFECH}]} = \frac{\Delta A_{\text{Absorbance at 421 nm}}}{\Delta A_{max}} \tag{7}$$

$$[\mathrm{BsFECH}]_{\mathrm{free}} = [\mathrm{BsFECH}]_0 - [\mathrm{BsFECH, TPPS}] \tag{8}$$

$$[\mathrm{BsFECH}]_{\mathrm{free}} = [\mathrm{BsFECH}]_0 - \alpha[\mathrm{TPPS}]_0 \tag{9}$$

where α is the ratio of concentration of the complexed TPPS denoted by [BsFECH,TPPS] as plotted *versus* the concentration of TPPS. ΔAbsorbance at 421 nm is the variation of absorbance at 421 nm upon titration with BsFECH and ΔA_{max} is the maximum change in the absorption intensity at 421 nm when TPPS is saturated with FECH.

3.4. Kinetics of insertion of zinc(II) in TPPS

In the presence of excess of Zn(II), the UV-vis absorption spectrum of TPPS changes in the absence or in the presence of BsFECH to reach a common product but with different rates, as may be seen in Fig. 2. For conditions of constant enzyme concentration, [BsFECH] = 40 μM, in excess relative to [TPPS] = 1 μM, BsFECH binds TPPS:

$$\mathrm{BsFECH} + \mathrm{TPPS} \rightleftharpoons [\mathrm{BsFECH, TPPS}] \tag{10}$$

and the TPPS, BsFECH complex become the reactant for Zn(II):

$$\mathrm{Zn(II)} + [\mathrm{BsFECH, TPPS}] \overset{K_{binding}}{\rightleftharpoons} [\mathrm{Zn(II), BsFECH, TPPS}] \tag{11}$$

forming a tertiary complex as the final reactant for the catalytic reaction:

$$[\mathrm{Zn(II), BsFECH, TPPS}] \overset{k_2}{\rightarrow} \mathrm{ZnTPPS} + \mathrm{BsFECH} \tag{12}$$

Under the actual conditions, the rate of formation of ZnTPPS will follow the rate law (Beringer & Gindler, 1955)

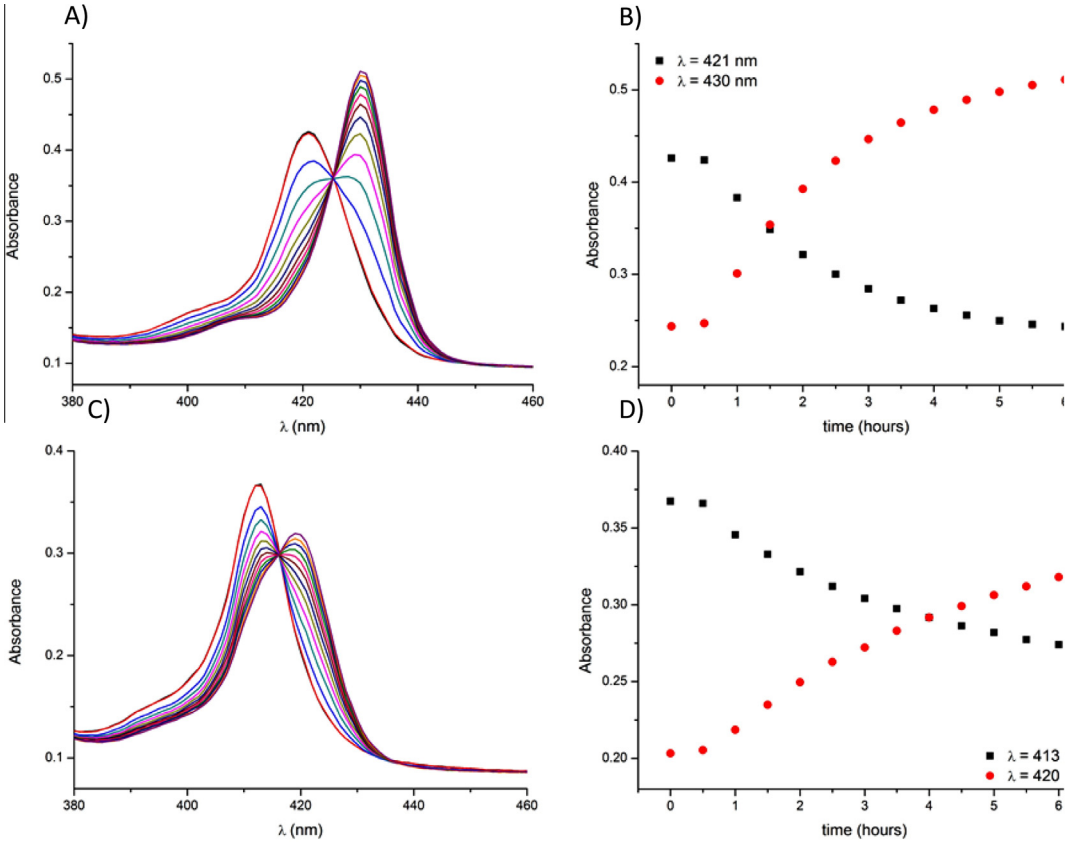

Fig. 2. Catalysed and non-catalyzed reaction between Zn(II) (100 μM) and TPPS (1.0 μM) in aqueous solution of pH 5.7 with 200 mM NaCl at 30 °C. A) Spectral changes for 40 μM FECH. B) Absorbance time traces at 421 nm (decay) and 430 (growth) for spectral changes in A. C) and D) non-catalyzed reaction for same conditions as in A and B with decay curve for 413 nm and growth at 420 nm.

$$-\frac{d[TPPS, BsFECH]}{dt} = k_{obs} * [TPPS, BsFECH] \quad (13)$$

where

$$k_{obs} = \frac{k_2 * K_{binding} * [Zn(II)]}{1 + K_{binding} * [Zn(II)]} \quad (14)$$

The time traces for decay of TPPS and the formation of Zn(TPPS) complex as seen in Fig. 2 corresponds to first-order kinetics in agreement with a rate determining intramolecular step following a fast bimolecular complex formation. Values for k_{obs} (s^{-1}) are reported in Table S1 (Supplementary information).

The observed first-order rate constant, k_{obs}, are increasing with rising concentration of Zn(II) ions but is approaching a limiting value as may be seen from Fig. 3. This dependence corresponds to Eq. (14) and the limiting rate is determined by k_2 for the unimolecular decay of the tertiary [Zn(II),BsFECH,TPPS] complex. For the actual conditions, $k_2 = 6.6 \pm 0.03$ 10^{-1} s^{-1} and $K_{binding} = 1.3 \pm 0.3$ 10^4 mo/L for binding of Zn(II) ions to the [TPPS, BsFECH] binary complex, were obtained by non-linear fitting, see Fig. 3.

The increasing rate for insertion of Zn(II) ions into TPPS as seen in Fig. 3 is accordingly concluded to be caused by binding of Zn(II) ions to TPPS bound to BsFECH. The binding of Zn(II) ions to the [TPPS,BsFECH] binary complex is comparable to binding of Zn(II) to bovine liver ferrochelatase as seen from the reported Michaelis-Menten constant for this enzyme with Zn(II) as substrate (Taketani & Tokunaga, 1982). Using TPPS as a model substrate accordingly showed that the catalytic activity of the recombinant BsFECH was preserved during purification and may be assigned to a binding of Zn(II) ions to the [TPPS,BsFECH] complex resulting in a rate enhancement due to a possible distortion of the porphyrin ring (Franco et al., 2000).

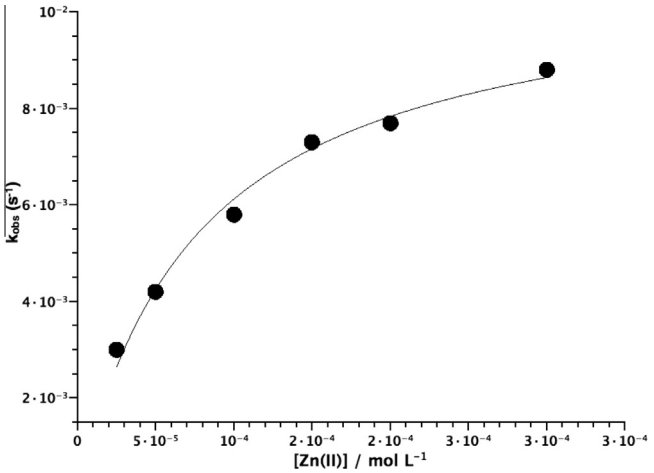

Fig. 3. Observed first-order rate constant for insertion of Zn(II) in TPPS in aqueous solution of pH 5.7 with 200 mM NaCl at 30 °C as function of excess concentration of Zn(II) in the presence of 40 μM FECH. Full line obtained by non-linear regression accordingly to Eq. (14).

3.5. Insertion of zinc ions in myoglobin

We have previously described a mechanism for Zn-protoporphyrin formation during Parma ham maturation,

which involves proteolysis and formation of low molecular weight peptides by proteolytic activity of endogenous chatepsins (Grossi et al., 2014). In order to test and confirm this hypothesis we first needed to show that recombinant BsFECH is active with ferrous myoglobin as substrate in presence of Zn(II) ions. Horse heart metmyoglobin was incubated with zinc for 24 h at 30 °C, with and without BsFECH in an oxygen free solution with excess of ascorbate added to obtain a reducing environment. From the fluorescence emission spectrum it is evident that BsFECH is active and is promoting removal of iron and insertion of zinc in the porphyrin ring forming a fluorescent zinc porphyrin (Fig. S4, Supplementary information). Circular dichroism (CD) spectroscopy was used to control that the incubation temperature was not affecting the native state of myoglobin and thus promoting transmetallation (Fig. S4, Supplementary information). From the CD spectra, no change of the native myoglobin structure at 30 °C is evident even after 12 h of incubation. These data taken together confirm optimal conditions for testing how partial proteolysis affects the iron/zinc transmetallation. Myoglobin was incubated with pepsin for different incubation times. In Fig. 4A, the SDS-PAGE electropherogram shows that myoglobin undergoes limited degradation when incubated for shorter periods of time (5–15 min.), whereas myoglobin is completely degraded after longer incubation time (30–120 min.). The same experimental condition as for the experiment shown in Fig. 4A were used for comparison of transmetallation in native myoglobin with myoglobin after different degree of pepsin degradation. From the results shown in Fig. 4B, it is clear that mild myoglobin proteolysis (5 and 10 min) provides a better substrate for iron/zinc transmetallation catalyzed by BsFECH, while longer incubation periods result in myoglobin degradation destroying myoglobin as substrate.

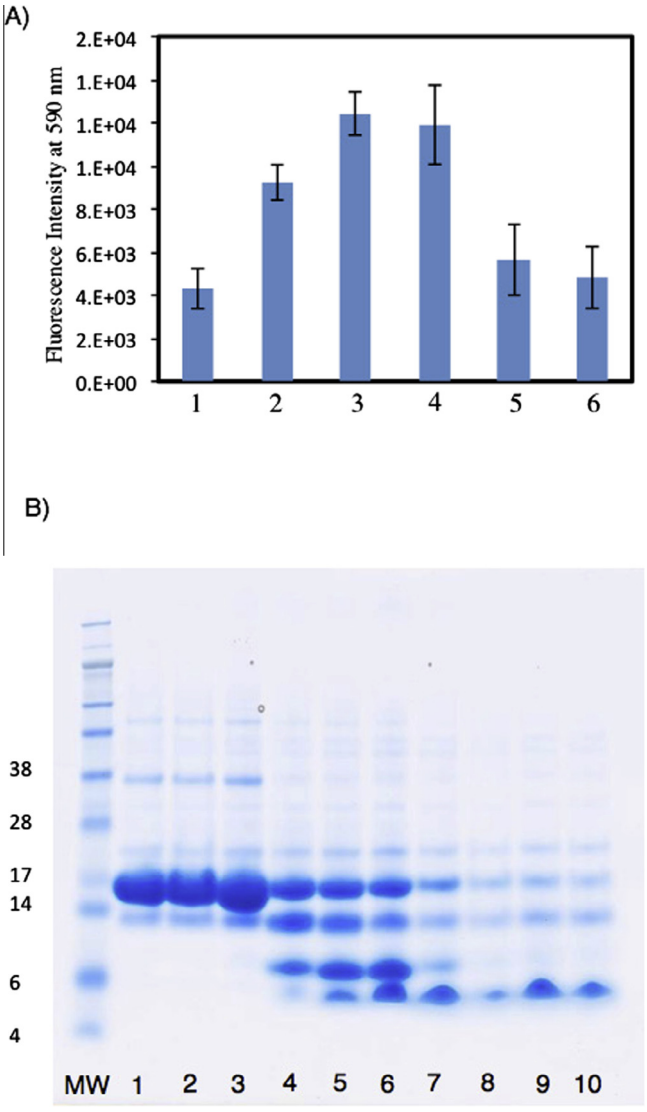

Fig. 4. A) Relative fluorescence intensity at 590 nm of myoglobin partly proteolyzed with pepsin in presence of 100 μM zinc acetate and 40 μM FECH: 1-without pepsin and without FECH, 2-without pepsin, 3-after 5 min of proteolysis, 4-after 10 min of proteolysis, 5-after 60 min proteolysis, and 6-after 90 min proteolysis. B) SDS PAGE 12%: 1-molecular weight markers, 2-myoglobin plus pepsin pH 7.4 time zero, 3-myoglobin plus pepsin pH 7.4 time zero, 4- myoglobin plus pepsin pH 7.4 time zero, 5–5 min proteolyzed myoglobin, 6–10 min proteolyzed myoglobin, 7–15 min proteolyzed myoglobin, 8–30 min proteolyzed myoglobin, and 9–60 min proteolyzed myoglobin, 10–120 min proteolyzed myoglobin.

For 5 min of digestion, LC–ESI-MS as shown in Fig. 5 indicates that two main partially proteolyzed proteins are formed with a MW of 13.8 kDa for the major component and 13.5 kDa for the minor component. These fragments are compatible with the partially proteolyzed myoglobin fragment with MW around 13 kDa analogous to the mini-myoglobin, which covers the 32–139 amino acid residues of myoglobin, and does not contain the helix A and part of helix B and H as are present in native myoglobin. The mini-myoglobin exhibit secondary and tertiary structures, and is shown to bind the heme group (Desanctis, Falcioni, Giardina, Ascoli, & Brunori, 1988). Our analysis indicate that the fragments observed in the LC–ESI-MS experiments are formed by proteolysis from the N-terminal region of horse heart myoglobin by pepsin, see Fig. 5, yielding fragments 29–153 and 32–153 in which the helix A and part of helix B were cleaved. The absence of A and part of B helices should destabilize the whole structure facilitating the FECH access to heme group. Further, using protein structure prediction by a homology/analogy recognition engine (Kelley & Sternberg, 2009) this "mini-myoglobin-like" fragment, which is capable of bind heme-iron (Desanctis et al., 1994), is seen from Fig. 5C to have a channel grating access to the heme center as compared to native myoglobin. This channel could provide a reaction path for a zinc/iron transmetallation reaction based on protein-protein interaction between the globin part of myoglobin and FECH.

Protein-protein interactions are a common initial step in many complex biological processes. The data presented in this work indicate that a direct interaction between myoglobin and FECH takes place. Chemical crosslinking using disuccinimidyl suberate (DSS) with a 11.2 Å arm as a bi-functional reagent for reaction with primary amines showed that myoglobin incubated with BsFECH react through direct contact as in evidenced by the 60 kDa band seen in the SDS-PAGE electropherogram (Fig. S5A, Supporting information). Additional evidence for the protein-protein interaction was obtained by a pull-down assay using BsFECH caring the His-tag as the bait protein (Ciruela et al., 2004). As may be seen at lane 4 of the 17.5% SDS-PAGE electropherogram in Fig. S5B (Supporting information), the bands corresponding to bait protein (BsFECH) and prey protein (metmyoglobin) is clearly seen after three sequential washes and elution from the Ni-affinity resin further confirming the existence of protein-protein interaction.

BsFECH-myoglobin interaction was investigated in more detail by isothermal titration calorimetry (ITC) aiming to provide the association constant, stoichiometry, and thermodynamic parameters for the protein-protein interaction. Fig. 6 shows the ITC titration curve (upper panel) and binding isotherm (lower panel) obtained for titrating BsFECH with metmyoglobin at 30 °C. The dilution heat of metmyoglobin was found by the titrating the metmyoglobin against the buffer and it was observed to be constant over all titration injections. Thus, by using the last five titrating injection points from Fig. 6 for dilution heat correction, a

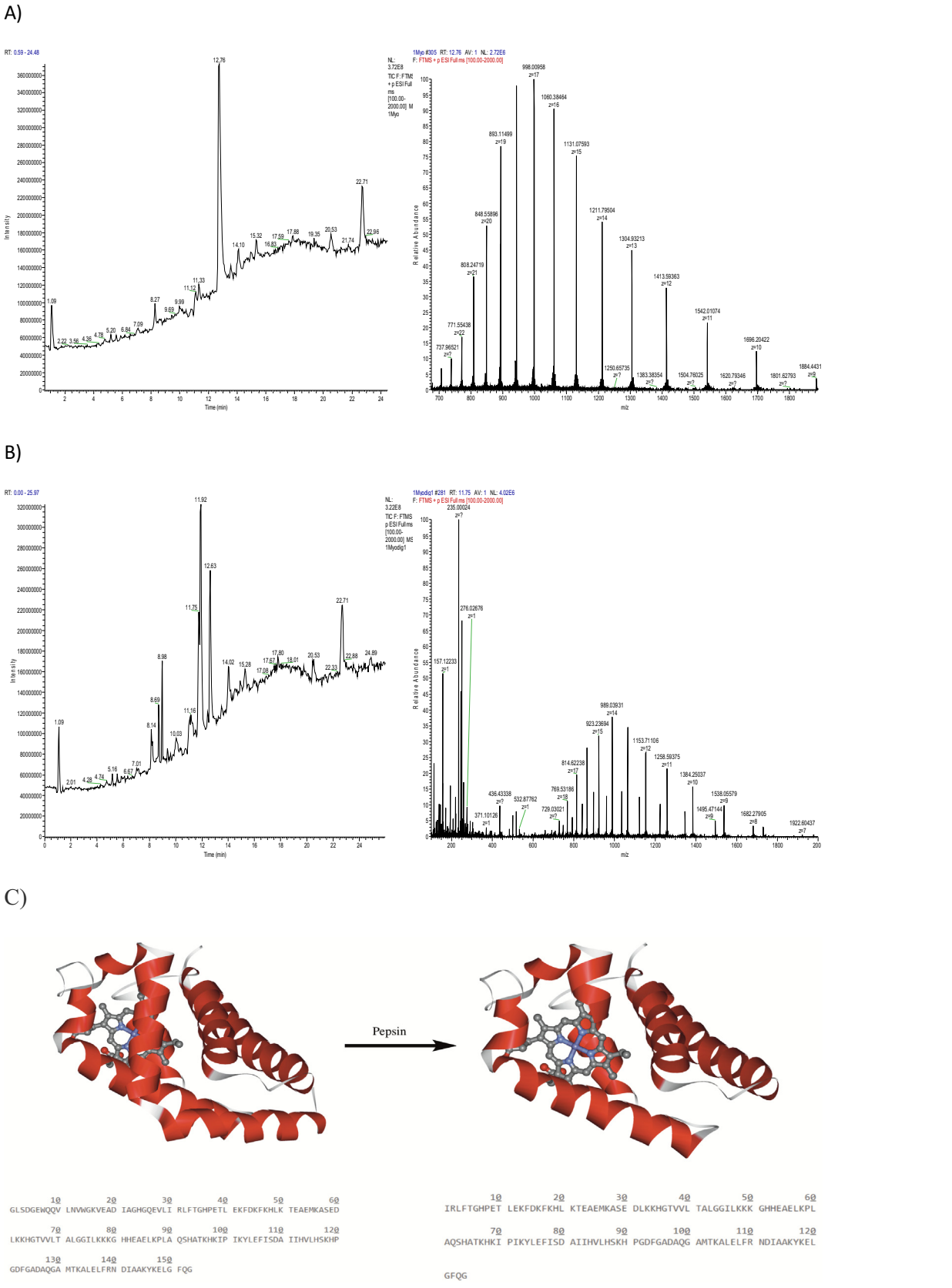

Fig. 5. A) LC–MS of aqueous solution of intact myoglobin (right panel) and high-resolution accurate ESI-MS spectrum for elution peak at 12.76 min yielding a MW of 16,951 Da for apomyoglobin after spectral deconvolution. B) LC–MS of aqueous solution of myoglobin after 5 min of proteolysis with pepsin (right panel) and high-resolution accurate ESI-MS spectrum for elution peak at 11.75 min provide evidence for a major peptide component with MW of 13,833 Da and a minor component with MW of 13,451 Da after spectral deconvolution. These myoglobin fragments are compatible with the myoglobin fragments 29–153 (predicted MW 13,834.0 Da) and 32–153 (predicted MW 13,451.5 Da), as predicted by the program Peptide Cutter (http://web.expasy.org/peptide_cutter/). C) Structure illustration and proposed amino acid sequence of myoglobin and the mini-myoglobin obtained after 5 min of pepsin proteolysis as shown by SDS-PAGE (Fig. 4) and LC–ESI-MS.

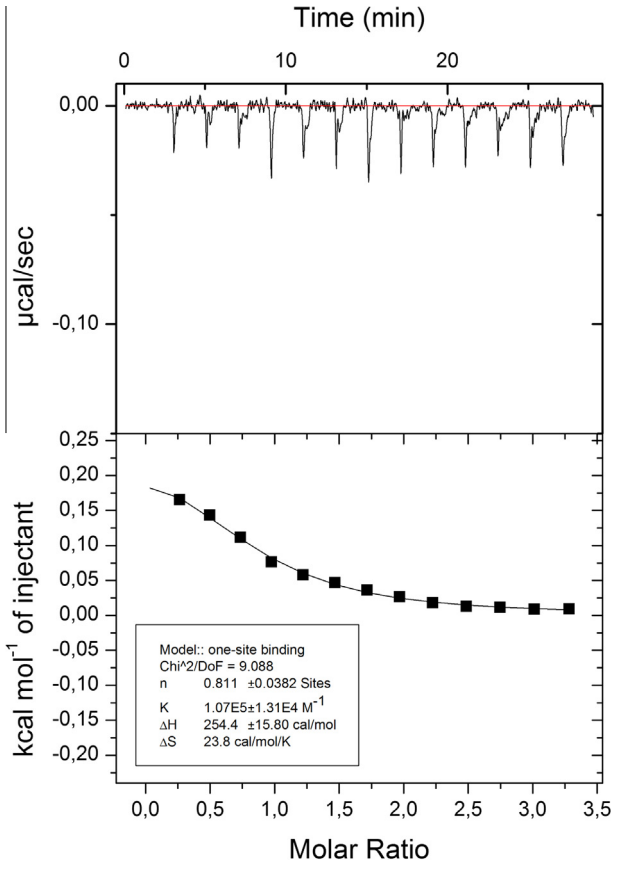

Fig. 6. ITC titration curve (upper panel) and binding isotherm (lower panel) obtained for titrating 203.8 µL of a 30 µM BsFECH solution with a 500 µM metmyoglobin solution using a initial injection of 0.4 µL and 13 injections of 2.8 µL in aqueous solution of pH 5.7 with 200 mM NaCl at 30 °C.

association constant of $1.07 \pm 0.13\ 10^5$ mol/L at 30 °C is obtained from the non-linear curve-fitting of the binding isotherm to one-site binding model equation ($n = 0.81 \pm 0.04$). The interaction of BsFECH and metmyoglobin exhibit a slightly endothermic character with $\Delta H_{apparent} = 0.25 \pm 0.02$ kcal/mol and an apparent ΔC_p close to zero. Fig. S6 (Supporting information) shows that the association constant for the BsFECH-myoglobin interaction slightly decrease with increasing temperature and is supported by the predominant entropic driven interaction ($\Delta S_{apparent} = 23.8$ cal/mol K).

4. Conclusion

Transmetallation, as relevant for formation of the zinc protophorphyrin IX pigment in Parma ham, is clearly promoted by ferrochelatase. Kinetic studies with tetraphenylphorphyrinsulfonate as a water-soluble model substrate showed a significant rate enhancement based on binding to the enzyme facilitating insertion of zinc ions. In myoglobin partly digested by proteolysis a channel seems to open up for transmetallation again facilitated by ferrochelatase. The metal-exchange reaction, important in Parma ham during the long maturation process, accordingly seems to depend on two factors: (i) a limited proteolysis of the globin of myoglobin followed by (ii) interaction of myoglobin and ferrochelatase. The inhibiting effect of nitrite and nitric oxide seen for formation of the Parma pigment in traditional meat curing could be assigned both by reaction of nitrite or nitric oxide with the sulfur cluster in the active site of eukaryotic ferrochelatase and/or by reaction of exposed thiols residues of proteolytic enzymes leading to protein post-translational modification halting mild proteolysis of myoglobin, which now has been shown to enhance the transmetallation reaction catalyzed by ferrochelatase.

Acknowledgements

This research is part of the bilateral Brazilian/Danish Food Science Research Program "BEAM – Bread and Meat for the Future" supported by FAPESP (Grant 2011/51555-7) and by the Danish Research Council for Strategic Research (Grant 11-116064). D.R.C. thanks the Brazilian National Research Council – CNPq for the research Grant (305385/2009-7) and FAPESP (EMU 2009/54040-8).

Appendix A. Supplementary data

Supplementary data associated with this article can be found, in the online version, at http://dx.doi.org/10.1016/j.foodchem.2016.04.109.

References

Ajioka, R. S., Phillips, J. D., & Kushner, J. P. (2006). Biosynthesis of heme in mammals. *Biochimica et Biophysica Acta-Molecular Cell Research, 1763*(7), 723–736.
Al-Karadaghi, S., Hansson, M., Nikonov, S., Jonsson, B., & Hederstedt, L. (1997). Crystal structure of ferrochelatase: The terminal enzyme in heme biosynthesis. *Structure, 5*(11), 1501–1510.
Barrios, D. A., D'Antonio, J., McCombs, N. L., Zhao, J., Franzen, S., Schmidt, A. C., ... Ghiladi, R. A. (2014). Peroxygenase and oxidase activities of dehaloperoxidase-hemoglobin from *Amphitrite ornata*. *Journal of the American Chemical Society, 136*(22), 7914–7925.
Becker, E. M., Westermann, S., Hansson, M., & Skibsted, L. H. (2012). Parallel enzymatic and non-enzymatic formation of zinc protoporphyrin IX in pork. *Food Chemistry, 130*(4), 832–840.
Beringer, F. M., & Gindler, E. M. (1955). Ion pairs as intermediates in irreversible reactions of electrolytes. *Journal of the American Chemical Society, 77*(12), 3200–3203.
Bohm, G., Muhr, R., & Jaenicke, R. (1992). Quantitative-analysis of protein far uv circular-dichroism spectra by neural networks. *Protein Engineering, 5*(3), 191–195.
Bryan, N. S., Alexander, D. D., Coughlin, J. R., Milkowski, A. L., & Boffetta, P. (2012). Ingested nitrate and nitrite and stomach cancer risk: An updated review. *Food and Chemical Toxicology, 50*(10), 3646–3665.
Carlsen, C. U., & Skibsted, L. H. (2004). Myoglobin species with enhanced prooxidative activity is formed during mild proteolysis by pepsin. *Journal of Agricultural and Food Chemistry, 52*(6), 1675–1681.
Chau, T. T., Ishigaki, M., Kataoka, T., & Taketani, S. (2010). Porcine ferrochelatase: The relationship between iron-removal reaction and the conversion of heme to Zn-protoporphyrin. *Bioscience Biotechnology and Biochemistry, 74*(7), 1415–1420.
Chau, T. T., Ishigaki, M., Kataoka, T., & Taketani, S. (2011). Ferrochelatase catalyzes the formation of Zn-protoporphyrin of dry-cured ham via the conversion reaction from heme in meat. *Journal of Agricultural and Food Chemistry, 59*(22), 12238–12245.
Chenprakhon, P., Sucharitakul, J., Panijpan, B., & Chaiyen, P. (2010). Measuring binding affinity of protein-ligand interaction using spectrophotometry: Binding of neutral red to riboflavin-binding protein. *Journal of Chemical Education, 87*(8), 829–831.
Ciruela, F., Burgueno, J., Casado, V., Canals, M., Marcellino, D., Goldberg, S. R., ... Woods, A. S. (2004). Combining mass spectrometry and pull-down techniques for the study of receptor heteromerization. Direct epitope-epitope electrostatic interactions between adenosine A(2A) and dopamine D-2 receptors. *Analytical Chemistry, 76*(18), 5354–5363.
Desanctis, G., Falcioni, G., Giardina, B., Ascoli, F., & Brunori, M. (1988). Mini-myoglobin – The structural significance of heme-ligand interactions. *Journal of Molecular Biology, 200*(4), 725–733.
Desanctis, G., Falcioni, G., Polizio, F., Desideri, A., Giardina, B., Ascoli, F., & Brunori, M. (1994). Mini-myoglobin – native-like folding of the no-derivative. *Biochimica et Biophysica Acta-Protein Structure and Molecular Enzymology, 1204*(1), 28–32.
Edelhoch, H. (1967). Spectroscopic determination of tryptophan and tyrosine in proteins. *Biochemistry, 6*(7). 1948-&.
Ferreira, G. C., Franco, R., Lloyd, S. G., Moura, I., Moura, J. J. G., & Huynh, B. H. (1995). Structure and function of ferrochelatase. *Journal of Bioenergetics and Biomembranes, 27*(2), 221–229.
Franco, R., Ma, J. G., Lu, Y., Ferreira, G. C., & Shelnutt, J. A. (2000). Porphyrin interactions with wild-type and mutant mouse ferrochelatase. *Biochemistry, 39*(10), 2517–2529.
Greenfield, N. J. (2006). Using circular dichroism spectra to estimate protein secondary structure. *Nature Protocols, 1*(6), 2876–2890.
Grossi, A. B., do Nascimento, E. S. P., Cardoso, D. R., & Skibsted, L. H. (2014). Proteolysis involvement in zinc-protoporphyrin IX formation during Parma ham maturation. *Food Research International, 56*, 252–259.

Kelley, L. A., & Sternberg, M. J. E. (2009). Protein structure prediction on the Web: A case study using the Phyre server. *Nature Protocols, 4*(3), 363–371.
Mirvish, S. S. (1995). Role of N-nitroso compounds (NOC) and N-nitrosation in etiology of gastric, esophageal, nasopharyngeal and bladder-cancer and contribution to cancer of known exposures to NOC. *Cancer Letters, 93*(1), 17–48.
Morita, H., Niu, J., Sakata, R., & Nagata, Y. (1996). Red pigment of Parma ham and bacterial influence on its formation. *Journal of Food Science, 61*(5), 1021–1023.
Parolari, G., Benedini, R., & Toscani, T. (2009). Color formation in nitrite-free dried hams as related to Zn-protoporphyrin IX and Zn-chelatase activity. *Journal of Food Science, 74*(6), C413–C418.
Pegg, R. B., & Shahidi, F. (1997). Unraveling the chemical identity of meat pigments. *Critical Reviews in Food Science and Nutrition, 37*(6), 561–589.
Semenyuk, A. V., & Svergun, D. I. (1991). GNOM – a program package for small-angle scattering data-processing. *Journal of Applied Crystallography, 24*, 537–540.
Taketani, S., Ishigaki, M., Mizutani, A., Uebayashi, M., Numata, M., Ohgari, Y., & Kitajima, S. (2007). Heme synthase (ferrochelatase) catalyzes the removal of iron from heme and demetalation of metalloporphyrins. *Biochemistry, 46*(51), 15054–15061.
Taketani, S., & Tokunaga, R. (1982). Purification and substrate-specificity of bovine liver-ferrochelatase. *European Journal of Biochemistry, 127*(3), 443–447.
Wakamatsu, J., Nishimura, T., & Hattori, A. (2004). A Zn-porphyrin complex contributes to bright red color in Parma ham. *Meat Science, 67*(1), 95–100.